PtdIns(3,4,5)P_3 is a regulator of myosin-X localization and filopodia formation

Laure Plantard[1,*], Antti Arjonen[2,3,*], John G. Lock[1,4], Ghasem Nurani[1], Johanna Ivaska[2,3,5] and Staffan Strömblad[1,4,‡]

[1]Center for Biosciences, Department of Biosciences and Nutrition, Karolinska Institutet, 14183 Huddinge, Sweden
[2]Medical Biotechnology, VTT Technical Research Centre of Finland, Turku 20520, Finland
[3]Turku Centre for Biotechnology, University of Turku, Turku 20520, Finland
[4]Breast Cancer Theme Center, Karolinska Institutet, 14183 Huddinge, Sweden
[5]Department of Biochemistry and Food Chemistry, University of Turku, Turku 20520, Finland
*These authors contributed equally to this work
‡Author for correspondence (staffan.stromblad@ki.se)

Accepted 14 July 2010
Journal of Cell Science 123, 3525-3534

doi:10.1242/jcs.069609

Summary

Phosphatidylinositol (3,4,5)-trisphosphate [PtdIns(3,4,5)P_3] is a key regulator of cell signaling that acts by recruiting proteins to the cell membrane, such as at the leading edge during cell migration. Here, we show that PtdIns (3,4,5)P_3 plays a central role in filopodia formation via the binding of myosin-X (Myo10), a potent promoter of filopodia. We found that the second pleckstrin homology domain (Myo10-PH2) of Myo10 specifically binds to PtdIns(3,4,5)P_3, and that disruption of this binding led to impairment of filopodia and partial re-localization of Myo10 to microtubule-associated Rab7-positive endosomal vesicles. Given that the localization of Myo10 was dynamically restored to filopodia upon reinstatement of PtdIns(3,4,5)P_3-binding, our results indicate that PtdIns(3,4,5)P_3 binding to the Myo10-PH2 domain is involved in Myo10 trafficking and regulation of filopodia dynamics.

Key words: Endosome, Filopodia, Myosin-X, PH domain, PtdIns(3,4,5)P_3

Introduction

Migrating cells display polarized structures such as lamellipodia and filopodia at their leading edge. The formation of lamellipodia requires phosphatidylinositol (3,4,5)-trisphosphate [PtdIns(3,4,5)P_3] (Oikawa et al., 2004), a membrane lipid that localizes to the leading edge of migrating cells in a tightly regulated manner and is linked to actin cytoskeleton remodeling (Chen et al., 2003; Insall and Weiner, 2001; Nishio et al., 2007). PtdIns(3,4,5)P_3 was also reported to be enriched at the tip of dendritic filopodia (Luikart et al., 2008). The role of PtdIns(3,4,5)P_3 in cell migration is evident because disruption of PtdIns(3,4,5)P_3 metabolism impairs motility, potentially by inhibiting the specific recruitment of proteins to the leading edge (Nishio et al., 2007). Conversely, the role of phosphoinositides (PIs) in filopodia formation has remained unclear, although filopodia are functionally involved in cell migration and in important physiological events such as angiogenesis, neuronal growth cone formation and phagocytosis (Cox et al., 2002; Dent et al., 2007; Gerhardt et al., 2003). PtdIns(3,4,5)P_3 participates in the membrane recruitment of proteins via interaction with PI-binding domains such as pleckstrin homology (PH) domains (Halet, 2005). Although most PH domains exhibit unspecific binding properties to PIs (Lemmon and Ferguson, 2000), some are described as being highly specific (Lemmon et al., 1995; Varnai et al., 1999). For example, PLCδ1 and Btk PH domains specifically bind to PtdIns(4,5)P_2 and PtdIns(3,4,5)P_3, respectively. A few PH domains are also involved in protein–protein interactions (Cohen et al., 2007; Zhu et al., 2007a).

Myosin-X (Myo10) is an actin binding motor possessing three PH domains (Berg et al., 2000). Myo10 also associates with regions of dynamic actin (Berg et al., 2000), is recruited to phagocytic cups in a phosphoinositide 3-kinase (PI3K)-dependent manner (Cox et al., 2002), and plays a role in spindle formation during cell division (Toyoshima and Nishida, 2007; Weber et al., 2004; Woolner et al., 2008). Myo10 localizes to the tip of filopodia, at least in part owing to its ability to specifically bind bundled actin, and undergoes intrafilopodial motility both towards and from the filopodia tips (Berg and Cheney, 2002; Kerber et al., 2009; Nagy et al., 2008). Myo10 also promotes filopodia formation and/or stabilization (Bohil et al., 2006; Zhang et al., 2004) and conveys β-integrins and netrin (Zhang et al., 2004; Zhu et al., 2007b) to the tip of filopodia. However, it remains unclear by which mechanisms Myo10 can promote filopodia. Although dimerization of the Myo10 head, neck and coiled-coil domains has been suggested to be required for Myo10-induced filopodia promotion (Tokuo et al., 2007), it is still not clear whether the full-length Myo10 protein actually dimerizes (Knight et al., 2005).

Myo10 contains three distinct PH domains, but the potential specificity of Myo10-PH-domain-binding to PIs and the potential role of PI-binding in Myo10 function are not known in detail. Two recent screenings aiming at isolating PH domains that bind to PI3K products [PtdIns(3,4)P_2 and PtdIns(3,4,5)P_3] identified Myo10 as one of the proteins binding to PI3K products, although it was not clear whether Myo10 might bind PtdIns(3,4)P_2 and/or PtdIns(3,4,5)P_3 in these screens (Isakoff et al., 1998; Park et al., 2008). Here, we show that PtdIns(3,4,5)P_3 plays an important role in filopodia induction via binding to Myo10. We demonstrate that the second PH domain of Myo10 (Myo10-PH2) specifically binds to PtdIns(3,4,5)P_3 and no other PI, although Myo10-PH1 and Myo10-PH3 showed no binding to any tested lipids. Upon disruption of Myo10 binding to PtdIns(3,4,5)P_3, either by mutation of Myo10 or by inhibition of PtdIns(3,4,5)P_3 synthesis, Myo10 partially re-localized from filopodia tips to Rab7-positive vesicles

moving along microtubules. Notably, Myo10 localization was reverted from vesicles to filopodia upon restoration of PtdIns(3,4,5)P_3 synthesis, suggesting that PtdIns(3,4,5)P_3 might regulate Myo10 intracellular trafficking. Myo10 binding to PtdIns(3,4,5)P_3 also contributes to Myo10-induced increases in filopodia number. Taken together, these results indicate that PtdIns(3,4,5)P_3 binding regulates Myo10 trafficking and filopodia dynamics.

Results

Myo10 intracellular localization is influenced by its PH domains

The Myo10 domain structure is highly conserved, and includes three PH domains (Fig. 1A; supplementary material Fig. S1). Interestingly, although a construct of mCherry fused to wild-type Myo10 (mCherry–Myo10WT) localized at filopodia tips, deletion of all three Myo10 PH domains caused the partial re-localization of Myo10 to cytosolic puncta (Fig. 1B). Confocal microscopy showed that these puncta were indeed intracellular and not dorsal or ventral filopodia (Fig. 1B). This suggests that the PH domains of Myo10 are important in regulating Myo10 localization.

PtdIns(3,4,5)P_3 binds to Myo10-PH2 domain

To determine the lipid-binding capacity of individual Myo10 PH domains, we purified each of the three Myo10 PH domains fused to maltose binding protein (MBP) (Fig. 2A; supplementary material Fig. S1) and subjected them to a lipid pull-down assay against eight different PIs. MBP-PH2 bound specifically to PtdIns(3,4,5)P_3, although MBP-PH1, MBP-PH3 and MBP control showed no binding to any of the PIs (Fig. 2B,C). The Myo10 tail (Myo10Tail), which includes all three PH domains, also bound to PtdIns(3,4,5)P_3 but this binding was lost upon deletion of PH2 (Fig. 2D,E).

PtdIns(3,4,5)P_3 binding regulates Myo10 localization

Upon observing that Myo10 deleted of its three PH domains was re-localized, we mutated conserved PH domain-residues (which in other PH domains are crucial for lipid binding) in each of the three PH domains of Myo10 (Fig. 3A; supplementary material Fig. S1 and Table S1). Expression levels of the different constructs were comparable (supplementary material Fig. S2A). Mutagenesis of the conserved residues in Myo10-PH1 (K1179A) and Myo10-PH3 (K1395A) did not result in altered Myo10 localization (Fig. 3A,B). However, Myo10-KK1215/6AA (Myo10PH2pm; bearing point mutations in Myo10-PH2) as well as Myo10 with deleted PH2 (Myo10ΔPH2), showed a similar punctate localization to that observed upon deletion of all three Myo10 PH domains (Fig. 3B; supplementary material Movies 1, 2). Coincident with the punctuate staining, Myo10-PH2 mutants were also targeted significantly less to the tips of filopodia (Fig. 3B,C). Thus, Myo10 localization at the tip of filopodia is regulated by the Myo10-PH2 domain.

We then replaced the Myo10-PH2 domain with well-characterized PH domains from Btk, PLCδ1 and TAPP1, which bind specifically to PtdIns(3,4,5)P_3, PtdIns(4,5)P_2 and PtdIns(3,4)P_2, respectively (Halet, 2005; Varnai and Balla, 2006) (Fig. 3A). Although replacement of Myo10-PH2 with PtdIns(3,4,5)P_3- or PtdIns(4,5)P_2-binding PH domains restored the localization from intracellular puncta to filopodial tips, introduction of a PtdIns(3,4)P_2-binding PH domain did not correct the mislocalization of Myo10ΔPH2 (Fig. 3D,E). This shows that binding to either PtdIns(3,4,5)P_3 or to PtdIns(4,5)P_2 can promote Myo10 localization to the tips of filopodia.

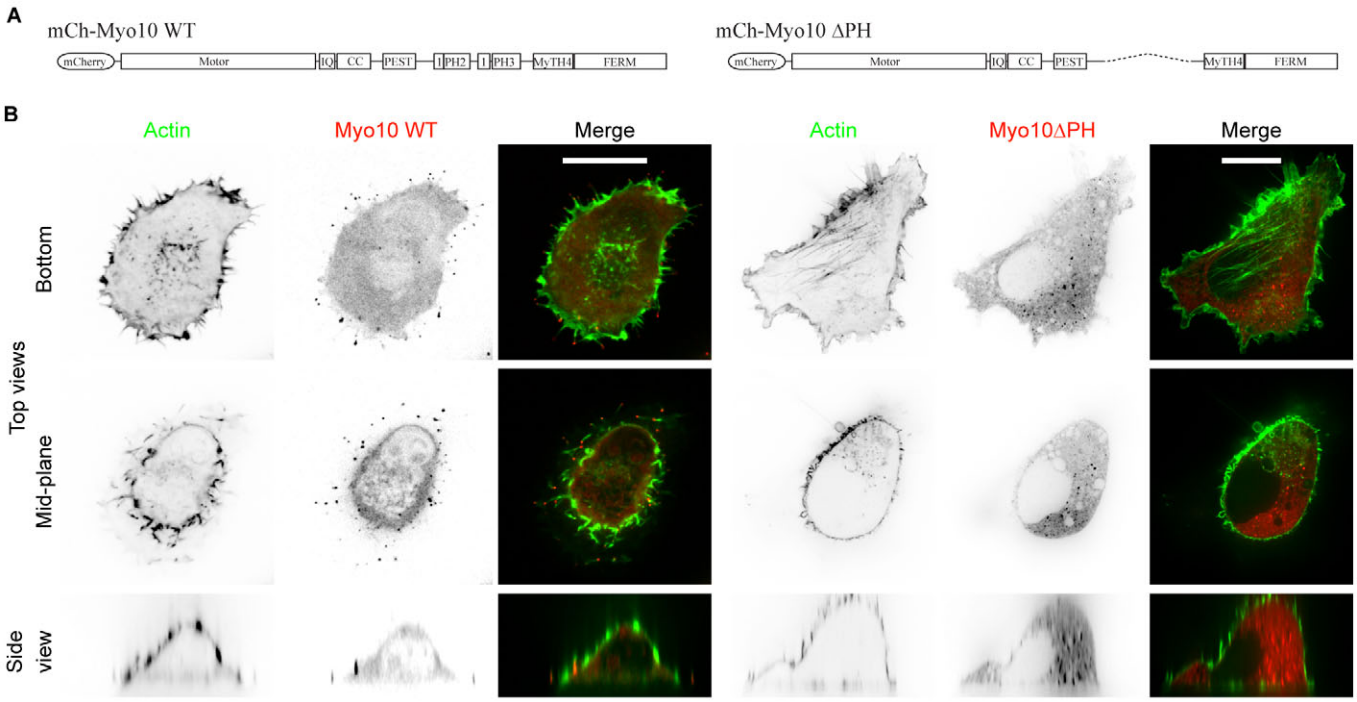

Fig. 1. Re-localization of Myo10 in the absence of PH domains. (**A**) Structure of constructs of Myo10WT and Myo10 with deleted PH domains, showing the different domains of the protein. (**B**) Mislocalization of Myo10 upon deletion of the three Myo10 PH domains. COS-7 cells transfected with mCherry–Myo10WT (red) and mCherry–Myo10ΔPH (red) were stained with Alexa-Fluor-488–Phalloidin (green). Single-colour images are shown as inverted contrast images. Top views are shown of the bottom and a mid plane, and side views of a single x–y slice, with individual channels and channels merged. Scale bars: 10 μm.

Complex formation containing more than one Myo10 molecule

We then examined whether different molecules of Myo10 could form complexes. We co-transfected COS-7 cells with either EGFP–Myo10WT and mCherry–Myo10WT or with EGFP–Myo10PH2pm and mCherry–Myo10ΔPH2 (Fig. 4A) and performed a co-immunoprecipitation with antibodies specific for either EGFP or mCherry (supplementary material Fig. S2B,C). The full-length Myo10WT co-immunoprecipitated with mCherry–Myo10WT (Fig. 4B, upper panel). In addition, mutation of the Myo10-PH2 domain had no effect on this association, because the two Myo10-PH2 mutant proteins also co-immunoprecipitated (Fig. 4B, lower panel). Furthermore, the presence of Myo10WT affected the localization of Myo10ΔPH2, because mCherry–Myo10ΔPH2 was localized at tips of filopodia to a higher degree when co-transfected with EGFP–Myo10WT than when co-transfected with EGFP (Fig. 4A,C). This indicates that different molecules of Myo10 do associate and that Myo10WT can bring the mutant Myo10ΔPH2 to filopodia tips. Notably, this might explain the detectable though substantially weaker localization of Myo10ΔPH2 to filopodia tips in singly transfected cells, because endogenous Myo10 is also present in these cells. Thus, the observed localization of Myo10 PH2 mutants in filopodia might result from association with endogenous Myo10 rather than from direct independent targeting.

Inhibition of PI3K reversibly re-localizes Myo10 to cytoplasmic puncta

Given the Myo10 re-localization upon mutation of its PtdIns(3,4,5)P_3 binding site, we next inhibited the production of PtdIns(3,4,5)P_3 using the PI3K inhibitors LY294002 and wortmannin in cells where filopodia were induced by overexpression of Myo10, and analyzed Myo10 localization (Fig. 5A,C,D; supplementary material Fig. S4, Movie 3). Efficient PI3K inhibition was controlled by Akt phosphorylation activity (Fig. 5B). After PI3K inhibition, mCherry–Myo10WT partially re-localized from the tips of filopodia to cytoplasmic puncta, similar to those labeled by mCherry–Myo10ΔPH2 (Fig. 5A,C,D). This effect was independent of the mCherry tag because the same effect was seen in cells transfected with EGFP–Myo10WT (supplementary material Movies 4, 5). The effects of the PI3K inhibitors on Myo10 localization were less prominent than those observed with the PH2-mutant forms of Myo10. These differences might arise because filopodia are formed in the presence of the Myo10-PH2 mutant under one experimental condition, although the effects on pre-existing filopodia are characterized in the case of short-term treatment with PI3K inhibitor. Nonetheless, wash-out of the PI3K inhibitor effectively restored Myo10 filopodial localization (Fig. 5E), suggesting that the puncta represent a transient re-localization of Myo10 in the absence of PtdIns(3,4,5)P_3 binding.

Myo10 localizes to endosomal vesicles in the absence of PtdIns(3,4,5)P_3 binding

We next performed more detailed analyses of the localization of Myo10-PH2 mutants as well as of Myo10WT in cells treated with PI3K inhibitors. First we noted that the Myo10-PH2 mutants were more soluble in cold Triton than PtdIns(3,4,5)P_3 binding Myo10 (supplementary material Fig. S3). Triton insolubility is frequently an indicator of cytoskeletal association (Fox, 1985; Quinn et al., 1989), and therefore this result suggests that PtdIns(3,4,5)P_3 binding to Myo10WT supports Myo10 binding to F-actin. We also found that the puncta of Myo10-PH2 mutants moved within the cell cytoplasm with top speeds of 0.33±0.05 μm/second, (Fig. 6A; supplementary material Fig. S4, Movies 6, 7), which correlates with previously published endosome velocities (Tacon et al., 2004). This movement was abolished by Nocodazole treatment (Fig. 6A). These results indicate that in the absence of PtdIns(3,4,5)P_3 binding, Myo10 localizes to vesicles moving along microtubules.

To characterize Myo10-positive vesicles, we co-labeled Myo10-expressing cells with endosomal and lysosomal markers (Fig. 6B; supplementary material Fig. S5). Interestingly, Myo10-KK1215/6AA PH2 colocalized partially with Rab7 and LAMP1 (Fig. 6B; supplementary material Fig. S5, Movie 8), but not with Rab4a, Rab5, Rab11 or Rab21 (supplementary material Fig. S5A), suggesting that Myo10 localized to late endosomal/lysosomal vesicles. Furthermore, overexpression of Rab7 together with

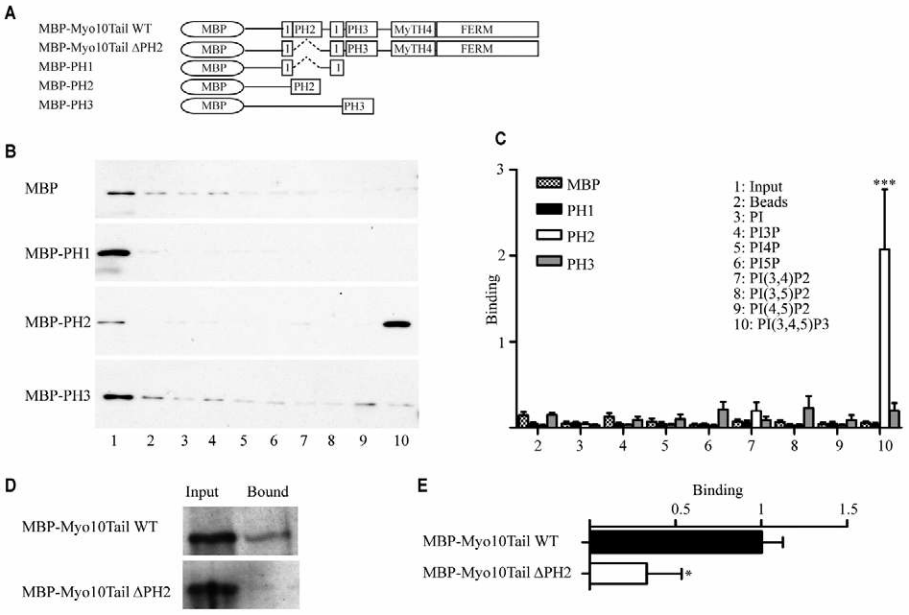

Fig. 2. Myo10 PH2 domain binds specifically to PtdIns(3,4,5)P_3. (**A**) Constructs allowing the expression of different domains of Myo10 fused to MBP for protein purification. (**B**) Purified MBP, MBP-PH1, MBP-PH2 and MBP-PH3 were subjected to a lipid pull-down assay with different PIs. After pull-down, immunoblot detected Myo10. The numbers below the gels correspond to the numbers in C. (**C**) Quantification of the binding of isolated PH1, PH2 and PH3 domains of Myo10 to lipids in a lipid pull-down assay. Comparison by Student's *t*-test (***P<0.001) to the MBP control. (**D**) MBP–Myo10TailWT but not MBP–Myo10TailΔPH2 binds to PtdIns(3,4,5)P_3. MBP–Myo10TailWT or MBP–Myo10TailΔPH2 were purified and subjected to immunoblotting after a PtdIns(3,4,5)P_3 pull-down. (**E**) The Myo10 tail binds to PtdIns(3,4,5)P_3 via its second PH domain (PH2). Quantification of the binding of MBP–Myo10TailWT and MBP–Myo10TailΔPH2 to PtdIns(3,4,5)P_3 in a lipid pull-down assay. Comparison by Student's *t*-test (*P<0.05). Graphs show means + s.e.m. of three independent experiments.

Myo10WT increased Myo10 localization to vesicles (Fig. 6B). In addition, endogenous Myo10 was localized in Rab7-positive vesicles, both in the presence of the PI3K inhibitor LY294002 and to a lower extent in its absence (supplementary material Fig. S5B). However, endogenous Myo10 was not found in LAMP1- or Rab21-positive vesicles (Fig. 6B; supplementary material Fig. S5) and

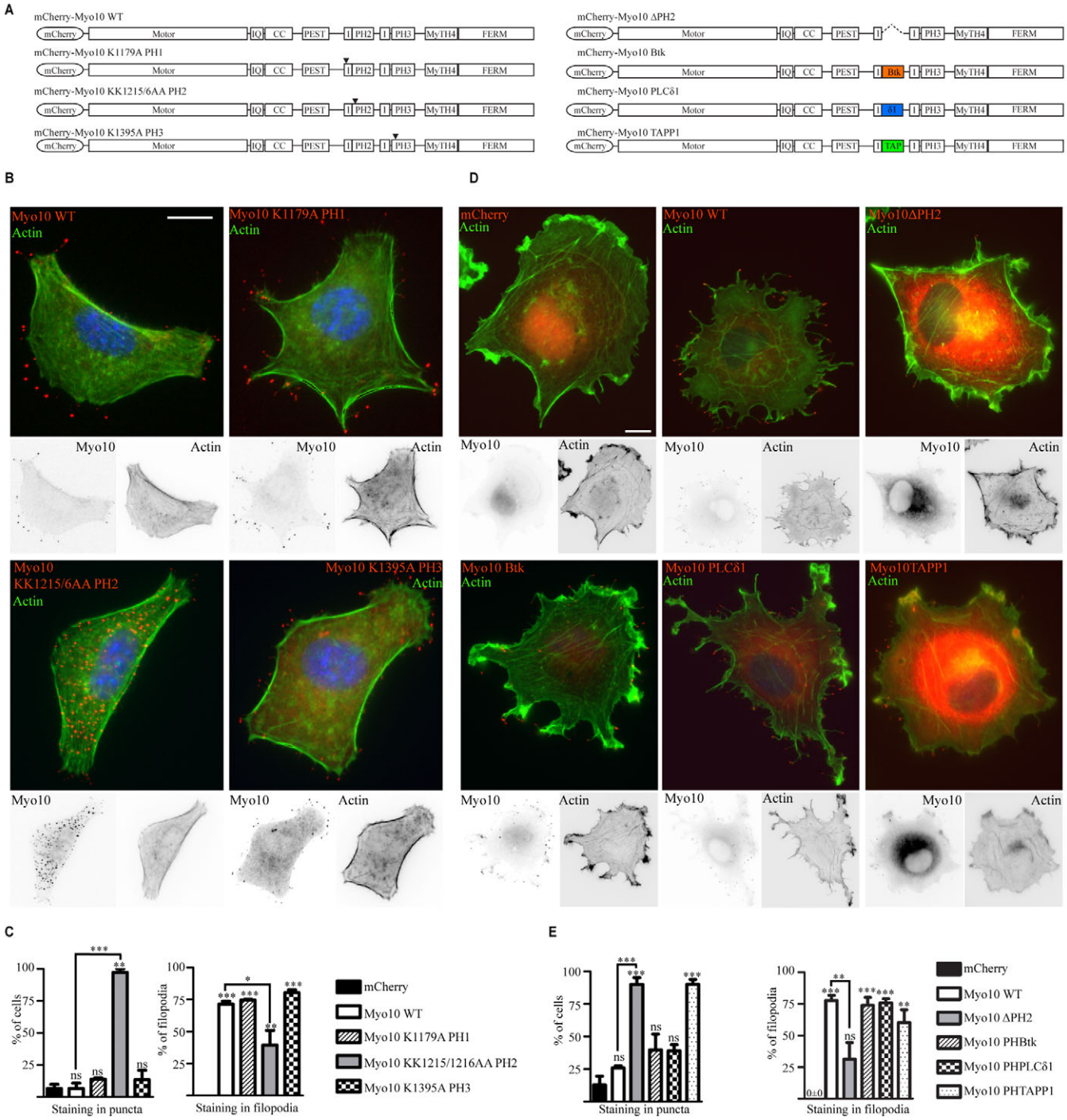

Fig. 3. PtdIns(3,4,5)P_3 regulates Myo10 localization. (**A**) mCherry–Myo10 constructs used in these experiments. (**B**) Mutations in the Myo10-PH2 domain lead to partial mislocalization of Myo10. HeLa cells transfected with mCherry–Myo10 constructs (red) and stained with FITC–phalloidin (green) and Hoechst 33342 (blue). Inverted contrast images for each of the channels are shown below each colour image in B and D. (**C**) The proportion of cells with Myo10 present in puncta and the proportion of filopodia with Myo10 at the tip were quantified. Analysis of 34–49 cells per condition in three independent experiments. (**D**) Binding to PtdIns(3,4,5)P_3 or PtdIns(4,5)P_2 can localize Myo10 at the tip of filopodia. COS-7 cells were transfected with mCherry, mCherry–Myo10WT, mCherry–Myo10ΔPH2, mCherry–Myo10Btk, mCherry–Myo10PLCδ1 or mCherry–Myo10TAPP1 (all red) and stained with FITC–phalloidin (green). (**E**) The proportion of cells with Myo10 present in puncta and the proportion of filopodia with Myo10 at the tip were quantified. Analysis of 42–68 cells per condition in three independent experiments. Graphs show means + s.e.m. Comparison by Student's *t*-test (ns, not significant; **P*<0.05, ***P*<0.01, ****P*< 0.001) to the mCherry control as indicated on top of bars and to mCherry–Myo10WT as indicated by brackets. Scale bars: 10 µm.

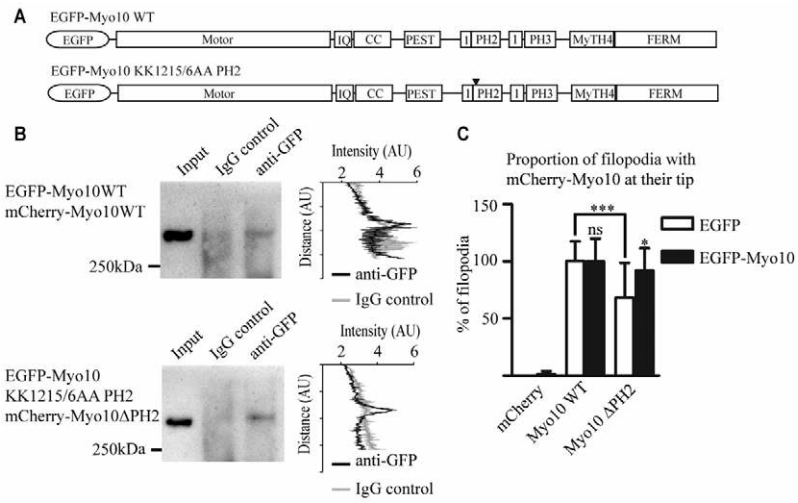

Fig. 4. Intracellular complex formation of more than one Myo10 molecule. (**A**) EGFP–Myo10 constructs. (**B**) Different full-length Myo10 molecules co-immunoprecipitate independently of PtdIns(3,4,5)P_3 binding. Co-immunoprecipitations were performed with anti-EGFP antibodies using COS-7 cells co-transfected with either mCherry–Myo10WT and EGFP–Myo10WT or with mCherry–Myo10ΔPH2 and GFP–Myo10PH2pm. Immunoprecipitates were then resolved by SDS-PAGE and analyzed by detecting mCherry with an anti-RFP antibody. The signal intensity was measured along three lines per lane on the western blot and plotted as mean + s.d. The gray and black lines represent, respectively, the IgG control and the precipitation by the anti-GFP antibody. (**C**) Myo10WT can relocate Myo10ΔPH2 to tips of filopodia. COS-7 cells were transfected with mCherry, mCherry–Myo10WT or mCherry–Myo10ΔPH2 in the presence of either EGFP or EGFP–Myo10WT. The proportion of filopodia with mCherry at their tip was quantified. Analysis of 43–52 cells per condition in three independent experiments. Graph shows means + s.e.m. Comparison by Student's *t*-test (ns, not significant; *P<0.05, **P<0.01, ***P<0.001) to the EGFP control as indicated on top of bars or to mCherry–Myo10WT as indicated by brackets.

therefore we cannot exclude the possibility that the observed localization of the mCherry–Myo10-PH2 mutant to lysosomes might be an artifact of protein overexpression. We also found that Myo10 and Rab7 double-positive vesicles undergo dynamic movements close to the cell membrane, as shown by total internal reflection fluorescence microscopy (TIRFM) (Fig. 6C; supplementary material Movie 9). This is in line with a previous report describing Rab7 recruitment to clathrin-coated structures at the plasma membrane (Barroso-Gonzalez et al., 2009). Thus, in the absence of PtdIns(3,4,5)P_3 binding, Myo10 predominantly localizes to endosomal vesicles trafficking close to the plasma membrane, suggesting that Myo10 might be transported to the plasma membrane via Rab7-containing vesicles.

PtdIns(3,4,5)P_3 binding is necessary for Myo10 promotion of filopodia

Myo10 induces filopodia in various mammalian cells (Berg and Cheney, 2002; Bohil et al., 2006; Zhang et al., 2004). Because Myo10 defective in PtdIns(3,4,5)P_3 binding was partially re-localized from filopodia, we analyzed whether the binding of PtdIns(3,4,5)P_3 to Myo10 affected its function in filopodia promotion. Although mCherry–Myo10WT, mCherry–Myo10-K1179A (PH1 mutant) and mCherry–Myo10-K1395A (PH3 mutant) transfected cells displayed a large increase in filopodia number in comparison to cells expressing mCherry control, the mCherry–Myo10-KK1215/6AA (PH2 mutant) and mCherry–Myo10ΔPH did not (Fig. 7A,B). mCherry–Myo10Btk and mCherry–Myo10PLCδ1 also promoted filopodia number although mCherry–Myo10ΔPH2 and mCherry–Myo10TAPP1 failed to induce filopodia (Fig. 7C). Thus, Myo10 promoted filopodia only when it was able to bind PtdIns(3,4,5)P_3 or PtdIns(4,5)P_2. In addition, a short treatment with PI3K inhibitor was able to decrease the number of filopodia in mCherry–Myo10WT transfected cells (Fig. 7D). Expression of mCherry–Myo10WT also caused an increase in filopodia length, although expression of mCherry–Myo10ΔPH2 did not (Fig. 7E). In conclusion, disruption of Myo10–PtdIns(3,4,5)P_3 binding impaired the capacity of Myo10 to promote filopodia number and length.

Discussion

We demonstrate here that the Myo10-PH2 domain binds specifically to PtdIns(3,4,5)P_3 and that this binding is important for Myo10 localization and function. Myo10 localization to the tip of filopodia is dependent on its head, neck and coiled-coil domains (HMM construct), with the motor domain binding to actin bundles and allowing the protein to reach the tip of filopodia (Berg and Cheney, 2002). Myo10 dimerization is also required for the motor domain to get to the tip of filopodia (Tokuo et al., 2007). These conclusions on the role for the Myo10 HMM region in Myo10 localization are based upon the use of Myo10 constructs lacking the tail (PH, MyTH4 and FERM domains). Although the Myo10 head, neck and coiled-coil domains are sufficient for filopodial tip localization, the full-length Myo10 constructs possessed additional domains that obviously contribute additional localization-regulating properties. Indeed, a construct corresponding to the three PH domains of Myo10 has also been indicated to localize at the plasma membrane (Mashanov et al., 2004).We therefore conclude that the C-terminal tail of Myo10 also contributes to Myo10 localization by binding to the membrane lipid PtdIns(3,4,5)P_3.

We demonstrate that different molecules of full-length Myo10 can associate, which is consistent with dimerization of Myo10 (Tokuo et al., 2007). Myo10 dimerization might be required for its motor activity (Tokuo et al., 2007). Although Myo10 in solution appears to be mainly monomeric (Knight et al., 2005), the head domain has been reported to dimerize when two molecules are in close vicinity (Sun et al., 2010). One hypothesis concerning the

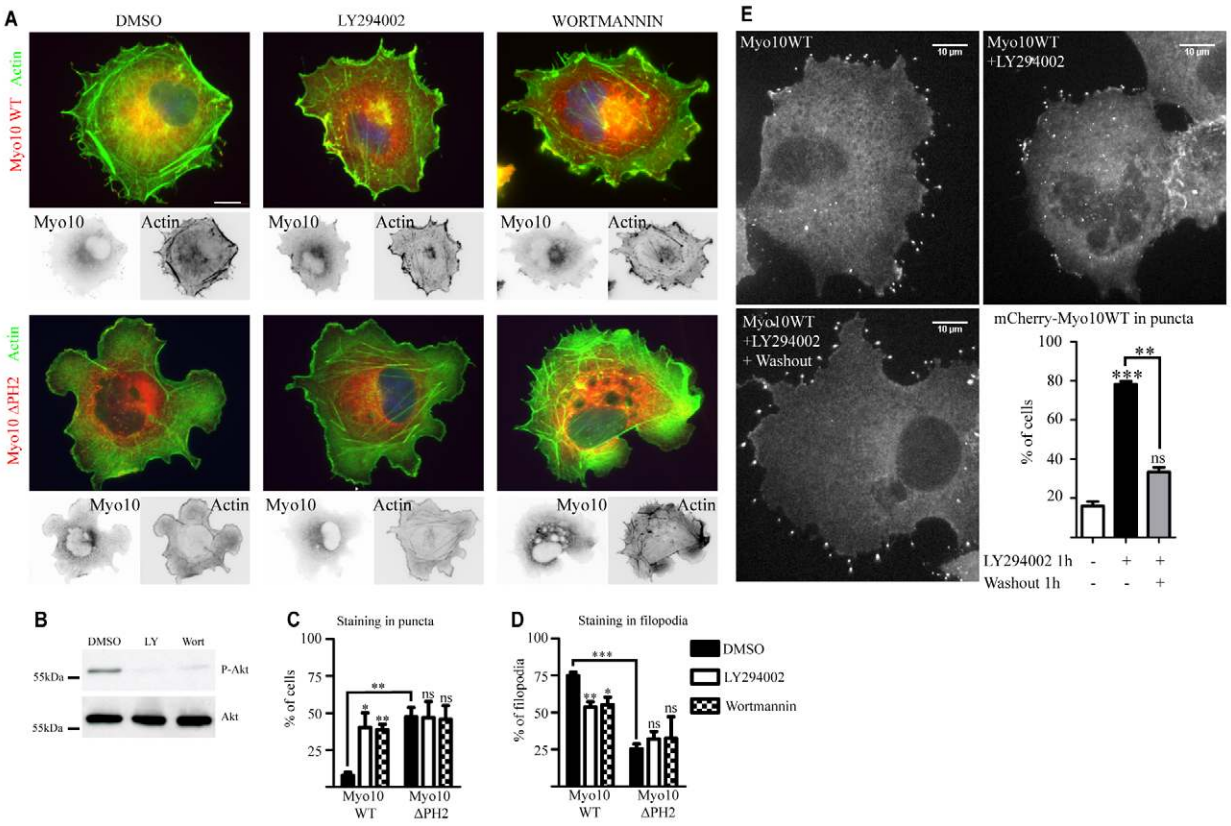

Fig. 5. Myo10 is reversibly re-localized upon inhibition of PI3K. (**A**) Myo10WT re-localization from filopodia tips to cytoplasmic puncta upon PI3K inhibition. COS-7 cells expressing mCherry–Myo10WT (red) were treated with DMSO, LY294002 or wortmannin and stained with FITC–phalloidin (green) and Hoechst 33342 (blue). Inverted contrast images for each of the channels are shown below each double channel image. (**B**) PI3K inhibition was assessed by checking Akt phosphorylation using immunoblotting. (**C**) The proportion of cells with Myo10 present in puncta was quantified. Analysis of 58–90 cells per condition in three independent experiments.(**D**) The proportion of filopodia with Myo10 at the tip was quantified. Analysis of 58–90 cells per condition in three independent experiments. (**E**) Myo10 mislocalization was rescued by wash-out after PI3K inhibitor treatment. COS-7 cells were transfected with mCherry–Myo10WT and treated with the PI3K inhibitor LY294002 for 1 hour, and the inhibitor was then washed out. Bar graph shows the proportion of cells with Myo10 in puncta. Analysis of 50–58 cells per condition in three separate experiments. Graphs show means + s.e.m. Comparison by Student's *t*-test (ns, not significant; **P*<0.05, ***P*<0.01, ****P*<0.001) to the mCherry control as indicated on top of the bars or as indicated by brackets. Scale bars: 10 µm.

regulation of Myo10 dimerization is that Myo10 might dimerize upon cargo binding, just like MyoVI (Yu et al., 2009). However, another motor protein, KIF1A, dimerizes only upon binding to PtdIns(4,5)P_2 (Klopfenstein et al., 2002). Our results are consistent with the dimerization of Myo10 being regulated independently of its PtdIns(3,4,5)P_3 binding.

In addition, we reveal that Myo10, when unable to bind to PtdIns(3,4,5)P_3, is localized in Rab-7-positive endosomal vesicles. This is consistent with earlier observations of a small amount of Myo10WT being located in intracellular puncta (Berg et al., 2000). Because we showed that this vesicular localization was reversible (Fig. 5E), and that the vesicle motion was microtubule-dependent, the endosomal localization of Myo10 might therefore be part of Myo10 trafficking or recycling pathways. The endocytic pathway has recently been described as an assembly platform implicated in actin dynamics and directed cell motility (Gould and Lippincott-Schwartz, 2009; Palamidessi et al., 2008). In a similar way, a machinery responsible for filopodia formation might be assembled on Rab-7-positive vesicles and might be activated upon PtdIns(3,4,5)P_3–Myo10 binding. Rab7 has been shown to be involved in phagocytosis and in phagosome fusion with late endosomes (Harrison et al., 2003). The formation of filopodia is a key step during phagocytosis, and Myo10 as well as PtdIns(3,4,5)P_3 have been shown to be important in phagocytosis (Cox et al., 2002; Niedergang and Chavrier, 2004). An interesting hypothesis is therefore that the Rab7-positive vesicles might be responsible for targeting Myo10 to sites of filopodia and/or phagocytotic cup formation.

We have also demonstrated that Myo10 unable to bind to PtdIns(3,4,5)P_3 was incapable of promoting filopodia, as is HMM–Myo10 (Berg and Cheney, 2002). The presence of the Myo10 tail is therefore required to increase the number and length of filopodia. Interestingly, a decrease in filopodia number has previously been reported in T cells treated by the PI3K inhibitor wortmannin (Johnson et al., 2008). In addition, as in our experiments, a recovery in filopodia number was observed after wortmannin washout (Johnson et al., 2008). Furthermore, inhibition of PI3K by LY294002 reduced filopodial motility in dendritic growth cones (Luikart et al., 2008). A decrease in filopodia merging rate has also been reported in a melanoma cell line treated with Nocodazole, which suggests that Nocodazole makes filopodia dynamically more stable (Schober et al., 2007). These reports are consistent with our findings on a role for PI3K in Myo10 trafficking and filopodia dynamics, and a role for microtubules in Myo10-labeled vesicle trafficking.

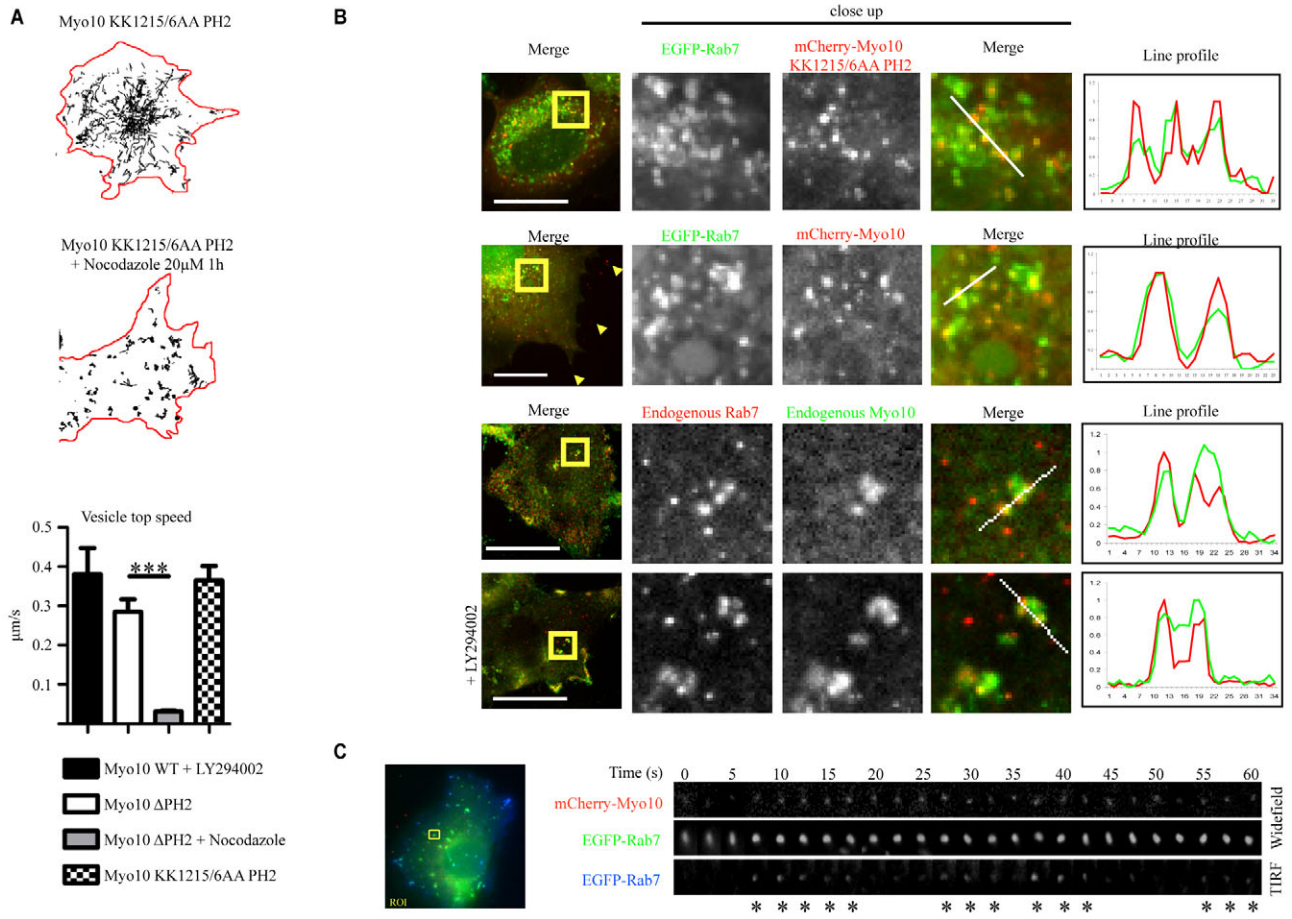

Fig. 6. Absence of PtdIns(3,4,5)P_3 binding localizes Myo10 to Rab7-positive vesicles. (**A**) Myo10-KK1215/6AA PH2 shows microtubule-dependent vesicular movement in the cell body. Upper: mCherry–Myo10-KK1215/6AA PH2 transfected COS-7 cells with or without Nocodazol treatment were imaged over time, and trajectories of vesicle tracks are shown in black lines. The cell edge is shown by the red perimeter line. Lower: Bar graphs show the vesicle top speed measured by tracking. Graphs show means + s.e.m. Comparison by Student's *t*-test (***P<0.001). (**B**) Myo10-KK1215/6AA PH2 colocalizes with Rab7. COS-7 cells were transfected with mCherry–Myo10-KK1215/6AA PH2 or mCherry–Myo10WT and EGFP-Rab7 or were stained for endogenous Myo10 and Rab7 as indicated. Images were acquired with a confocal microscope using 0.7 μm optical slices. In close-ups, regions of interest (ROI) are shown and a pixel line profile is drawn over merged images to illustrate colocalization. Maximum intensity projections are shown. Myo10 in the filopodia tips show no colocalization with Rab7 (yellow arrowheads). (**C**) Myo10WT is transported close to the plasma membrane in Rab7-positive vesicles. TIRFM imaging shows time-lapse series of COS-7 cells co-transfected with EGFP–Rab7 and mCherry–Myo10WT. Cells were treated with LY294002 to induce the vesicular phenotype of Myo10WT. Three channels were acquired: red shows Myo10 in widefield microscopy, green shows Rab7 in widefield, and blue shows Rab7 in the TIRFM channel (<100 nm proximity to glass surface). An ROI is shown in the panel of images where a vesicle positive for both Myo10 and Rab7 is tracked over time. Vesicle appearance in the TIRFM channel (asterisk) indicates close proximity of the vesicle to the membrane. Scale bars: 10 μm.

PtdIns(3,4,5)P_3 has been implicated in the regulation of actin polymerization (Chen et al., 2003; Insall and Weiner, 2001), which is required at the tip of filopodia for their formation. PtdIns(3,4,5)P_3 was also reported to be enriched in dendritic filopodia (Luikart et al., 2008). The mechanism by which PtdIns(3,4,5)P_3 regulates Myo10 function remains unclear. However, our data support the possibility that PtdIns(3,4,5)P_3 provides an anchor to the membrane (Manna et al., 2008; Oikawa et al., 2004) that recruits Myo10 to the plasma membrane. Thereafter, Myo10 might be involved in transporting PtdIns(3,4,5)P_3 to filopodia tips where it might serve to promote actin polymerization. We also found that Myo10 mutants binding PtdIns(4,5)P_2 were correctly localized and could induce filopodia, suggesting that for filopodia dynamics, binding of PtdIns(3,4,5)P_3 and PtdIns(4,5)P_2 to Myo10 might be exchangeable. Membrane anchoring and actin remodeling are roles that both PtdIns(4,5)P_2 and PtdIns(3,4,5)P_3 can sustain.

We found no binding partners for Myo10-PH1 or Myo10-PH3 domains amongst the PIs tested. PH domains might have other binding targets in addition to PIs, including protein partners (Cohen et al., 2007; Lemmon, 2004; van Rossum et al., 2005; Zhu et al., 2007a). However, no particular phenotype was seen upon expression of Myo10-PH1 or Myo10-PH3 mutants in mammalian cells. The role of Myo10-PH1 and Myo10-PH3 domains therefore remains unclear. However, Myo10 has several roles in cells; not only is Myo10 implicated in filopodia formation, but also in phagocytosis (Cox et al., 2002) and in cell division (Toyoshima and Nishida, 2007; Weber et al., 2004; Woolner et al., 2008), and it is possible that PH1 and/or PH3 might have roles in these or other Myo10-driven events.

In conclusion, we have demonstrated that Myo10 binds specifically to PtdIns(3,4,5)P_3 through its second PH domain. Our results also provide new insights into Myo10 trafficking by showing

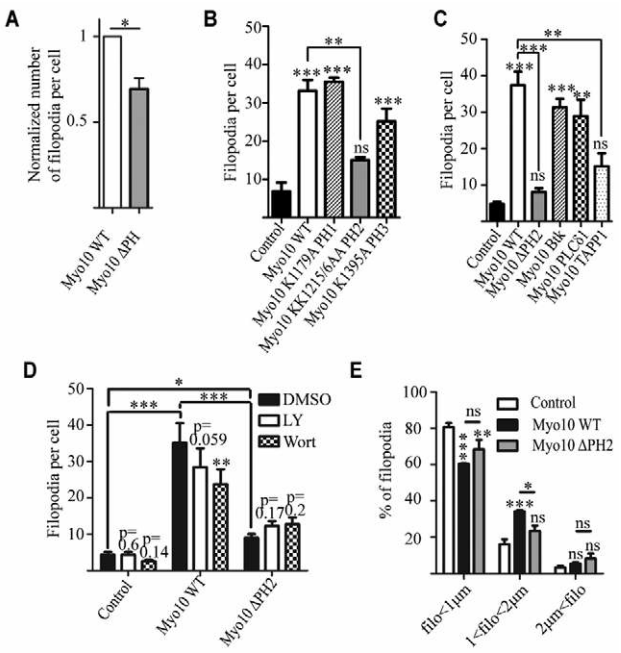

Fig. 7. Myo10-PH2 binding to PtdIns(3,4,5)P_3 is required for Myo10 function in filopodia. (**A**) Deletion of the three PH domains of Myo10 impairs filopodia. Cos-7 cells were transfected with mCherry–Myo10WT and mCherry–Myo10ΔPH. Bar graph shows the mean number of filopodia per cell normalized to Myo10WT transfected cells (n=3). (**B**) Mutation of Myo10-PH2 impairs filopodia. HeLa cells were transfected with mCherry, mCherry–Myo10WT, mCherry–Myo10-K1179A PH1, mCherry–Myo10-KK1215/6AA PH2 or mCherry–Myo10-K1395A PH3. Bar graph shows the number of filopodia per cell in 34–49 cells per condition in three experiments. (**C**) Myo10 binding to PtdIns(3,4,5)P_3 or PtdIns(4,5)P_2 promotes filopodia. COS-7 cells were transfected as in Fig. 2B prior to quantification of the number of filopodia per cell in 42–68 cells per condition in three experiments. (**D**) Inhibition of PI3K inhibits Myo10-induced filopodia. COS-7 cells expressing either mCherry, mCherry–Myo10WT or mCherry–Myo10ΔPH2 were treated for 1 hour with either DMSO, LY294002 or wortmannin. Quantification of filopodia number per cell was performed in 58–90 cells per condition in three experiments. (**E**) PtdIns(3,4,5)P_3 binding is necessary for Myo10-induced increase in filopodia length. Filopodia length was measured in COS-7 cells expressing mCherry, mCherry–Myo10WT or mCherry–Myo10ΔPH2. Bar graph displays the proportion of filopodia shorter than 1.5 µm, between 1.5 µm and 2.5 µm, or longer than 2.5 µm, based on seven independent experiments. Graphs display means + s.e.m. Comparison by Student's t-test (ns, not significant; *P<0.05, **P<0.01, ***P<0.001) to the mCherry-control as indicated on top of the bars or as indicated by brackets.

that Myo10 can be localized to endosomal vesicles moving along microtubules. Overall, it is now clear that PtdIns(3,4,5)P_3 binding regulates not only Myo10 localization and trafficking but also the frequency and structure of filopodia.

Materials and Methods

DNA constructs

Myo10-PH2 (E1206-A1304), Myo10-PH3 (E1386-D1491) and Myo10 tail (R1160-R2052) were amplified by PCR (supplementary material Table S1 and Fig. S1) and cloned into pMalC2E (New England Bioloabs) within *Xba*I and *Hind*III restriction sites to fuse them in N-terminal with MBP. Myo10-PH1 was cloned by deleting PH2 (E1206-A1304) from a Myo10-PH1+PH2 construct (P1170-G1378) (supplementary material Fig. S1).

pmCherry–Myo10WT was constructed by substituting EGFP from pEGFP–Myo10 (Berg and Cheney, 2002) using mCherry amplified by PCR from pR-SETBmCherry (Shaner et al., 2004). Mutations in these constructs were created using Quickchange XL site-directed mutagenesis kit (Stratagene). Point mutations of Myo10 PH domains (Myo10-K1179A PH1, Myo10-KK1215/6AA PH2 and Myo10-K1395A PH3) were made thanks to primers introducing one or two point mutations into the lipid binding site (supplementary material Table S1 and Fig. S1). Primers were also designed to delete the second PH domain of Myo10 (E1206-A1304) while inserting a SpeI restriction site (supplementary material Table S1 and Fig. S1). The three PH domains (mCherry–Myo10ΔPH) were deleted (S1131-Y1472) by adding an *Age*I site by site-directed mutagenesis (see supplementary material Table S1) followed by digestion and re-ligation of the construct. Btk, PLCδ1 and TAPP1 PH domains were amplified by PCR (supplementary material Table S1) and introduced in the mCherry–Myo10ΔPH2 construct in place of PH2, creating three chimeras: mCherry–Myo10Btk, mCherry–Myo10PLCδ1 and mCherry–Myo10TAPP1. EGFP–Myo10-KK1215/6AA PH2 was constructed by introducing the KK1215/6AA mutations into EGFP–Myo10WT with the same primers as used for pmCherry–Myo10-KK1215/6AA PH2.

Plasmids encoding EGFP–Rab4, EGFP–Rab5a, EGFP–Rab7, EGFP–Rab11, EGFP–Rab21 and EGFP–TAPP1PH have been previously described (Barbero et al., 2002; Gomes et al., 2003; Lebrand et al., 2002; Marshall et al., 2002; Pellinen et al., 2006; Rzomp et al., 2003; Wilcke et al., 2000). Plamids encoding EGFP–BtkPH and EGFP–PLCδ1PH were kind gifts from Matthias Wymann (University of Basel, Switzerland). All primers are listed in supplementary material Table S1. All plasmid sequences were verified by sequencing prior to use. Nucleotide alignment shown in supplementary material Fig. S1 was performed using Clustal W and Clustral X (Larkin et al., 2007).

Cell culture and transfection

HeLa carcinoma cells were cultured in Dulbecco's modified Eagle's medium (DMEM) (Invitrogen) with 5% FBS. COS-7 African green monkey kidney cells and MDA-MB-231 breast adenocarcinoma cells were cultured in DMEM with 10% FBS. Mouse aortic endothelial (MAE) cells were cultured in RPMI (Invitrogen) with 10% FBS. All DNA constructs were transfected using Lipofectamine 2000 (Invitrogen) or Fugene6 (Roche) according to the manufacturer's protocol.

Antibodies and reagents

The following antibodies and dyes were used: anti-RFP (PM005, MBL), anti-α-tubulin (12G10, Developmental Studies Hybridoma Bank, Iowa), anti-actin (JLA20, Developmental Studies Hybridoma Bank, Iowa), anti-LAMP1 (Santa Cruz Biotechnology), MBP-Probe (N17, Santa Cruz Biotechnology), anti-GFP (Clontech), anti-Akt (Cell Signaling), anti-phospho-Akt (Ser473) (Cell Signaling), anti-Myo10 (2243.00.02, SDIX) and anti-Rab7 (Rab7-117, Abcam), rabbit IgG (Sigma), FITC–Phalloidin (Invitrogen), Hoechst 33342 (Sigma). Alexa-Fluor-680 and Alexa-Fluor-700 secondary antibodies (Invitrogen) were used in LI-COR's Odyssey Infrared Imaging System and horse radish peroxidase-conjugated secondary antibodies (Jackson ImmunoResearch Laboratories) were used for detection by chemiluminescence. Nocodazole (10 µM, 1 hour at 37°C) was used to depolymerize microtubules. LY294002 (Sigma) (10–20 µM, 1 hour at 37°C) and wortmannin (Sigma) (0.15 µM, 1 hour at 37°C) were used to inhibit PI3K.

Protein purification and lipid pull-down assay

Proteins were produced with pMalC2E constructs. Plasmid expression was induced by IPTG and the bacteria were grown for 1 hour at 37°C prior to lysis. The proteins were then purified on an Amylose column (New England Biolabs) in accordance with the manufacturer's protocol.

Lipid pull-down assay was performed with PIP beads (Echelon Biosciences) according to the manufacturer's protocol. Briefly, 25 µl of PIP bead slurry at 10 nM was incubated with 0.04 µg/µl of purified Myo10 PH domains for 3 hours at 4°C, and then washed in 10 mM HEPES pH 7.4, 150 mM NaCl and 0.25% NP-40. Proteins bound to the beads were eluted in SDS-sample buffer and resolved by SDS-PAGE. Immunoblotting was analyzed with a VersaDoc Imaging System (Bio-Rad). Binding, defined as the ratio between the intensity of the bound fraction and the intensity of the input, was calculated.

Microscopy techniques

For imaging of fixed cells, cells were plated on Ibitreat µ-Dish dishes (Integrrated Biodiagnostics) one day before transfection. Transfected cells were fixed 12–24 hours after transfection with 2% paraformaldehyde, permeabilized with Triton-X100 and blocked with 2% BSA/PBS. Alternatively, cells were replated 24 hours after transfection on glass coverslips and allowed to attach for 2 hours prior to fixation.

Primary antibodies were used with predetermined optimal concentrations of 5–10 µg/ml. The concentration of Alexa-Fluor-conjugated secondary antibodies (Invitrogen) was 5 µg/ml. Alexa-Fluor-conjugated and FITC-conjugated phalloidins (Invitrogen) were used for F-actin detection. Cells were imaged on an Olympus IX71 microscope with Olympus 63× oil/1.4NA objective and a CCD Hamamatsu camera.

In live-cell experiments, cells were plated on Ibitreat µ-Dish dishes (Integrrated Biodiagnostics) one day before transfection. Transfected cells were imaged 12–24

hours after transfection. To maintain optimal conditions, a cell culture dish heater, objective heater at 37°C and 4.8% CO_2 support were used. Confocal three-dimensional images were taken using Zeiss Axiovert 200M with spinning disc confocal unit Yokogawa CSU22 and Zeiss Plan-Neofluar 63× oil/1.4 NA objective. Z-stacks with 1 airy unit (approx. 0.7 μm) optical slices were acquired with a step size of 0.3–0.7 μm between slices.

In TIRFM, cells were plated as above on Mattek glass bottom dishes. An Olympus IX71 MT20 CellR system with 60× oil/1.45NA TIRFM objective, MWB2 TIRF/FITC filter block and a 488 nm laser line was used to acquire total internal reflection images and widefield epifluorescence images sequentially (University of Turku, Department of Cell Biology and Anatomy). The maximum intensity projections were created with SlideBook 4.2.0.7 software and NIH ImageJ. QuickTime movies from time-lapse experiments were created using NIH ImageJ software.

In live-cell experiments, transfected cells were imaged 12–24 hours after transfection. Confocal three-dimensional images were taken using Zeiss Axiovert 200M. For PtdIns(3,4,5)P_3 localization experiments, cells were imaged with a Zeiss LSM 510.

Image analysis

ImageJ plugin Particle Detector and Tracker (Sbalzarini and Koumoutsakos, 2005) was used to automatically detect, track and visualize vesicle trajectories in time-lapse movies. Also, manual tracking and plugin MTrackJ (Erik Meijering, University Medical Center, Rotterdam, The Netherlands) were used in tracking vesicles. Cell Counter (Kurt De Vos, University of Sheffield, Sheffield, UK) and Manual Tracking (Fabrice P. Cordelières, Institut Curie, Orsay, France) plugins were used to count filopodia and track cells, respectively. Standard ImageJ tools were used to draw line profiles and measure filopodia length as well as signal intensities. Quantitative analysis of colocalization was done with the help of ImageJ plugin JACoP (Bolte and Cordelieres, 2006). Costes' approach was used to calculate Pearson correlation coefficients in the whole cell level for endogenous Myo10, Rab7 and Rab21 (Costes et al., 2004).

Cold Triton fractionation

Cold Triton fractionation protocol was modified from a published method (Ding et al., 1996). Transfected COS-7 cells were washed and scraped in ice-cold cytoskeleton-stabilizing buffer (CSK buffer) containing: 250 mM sucrose, 3 mM MgCl2, 150 mM KCl, 1 mM EGTA and 1 mM PMSF in 10 mM PIPES, pH 6.8. After spinning-down at 7000 ***g*** for 5minutes at +4°C, the pellet was resuspended in ice-cold 0.2% Triton X-100 (Sigma) in CSK buffer with protease inhibitor cocktail (Complete, Roche) and incubated on ice for 20 minutes. After centrifugation at 15,000 ***g*** for 10 minutes, the supernatant was considered as a soluble fraction and the pellet was considered as an non-soluble fraction. Supernatant and pellet were analyzed with standard western blotting techniques and detected using the LI-COR Odyssey Infrared Imaging System. The protein load was balanced to the tubulin signal.

Co-immunoprecipitation

At 24 hours after transfection, cell lysates were prepared in RIPA buffer from COS-7 cells co-transfected either with EGFP–Myo10WT and mcherry–Myo10WT or with EGFP–Myo10-KK1215/6AA PH2 and mCherry–Myo10ΔPH2. Cell lysates were incubated in the presence of anti-GFP antibody. Protein G beads (Santa Cruz Biotechnology) were used to capture the beads to which the antibodies and proteins were bound. Samples extracts were resolved by SDS-PAGE and detected by immunoblotting with an anti-RFP antibody (MBL, Japan).

We thank Matthias P. Wymann (University of Basel, Switzerland) for the EGFP–BtkPH and EGFP–PLCδ1PH constructs; Richard E. Cheney (University of North Carolina at Chapel Hill, NC) for EGFP–bovMyo10; Aaron J. Marshall (University of Manitoba, Winnipeg, Canada) for EGFP–TAPP1PH; and Andew D. Paterson for assistance with microscopy. S.S. was supported by grants from the Swedish Cancer Society, the Swedish Research Council, and the Center for Biosciences at Karolinska Institutet. J.I. was supported by an ERC starting grant, Academy of Finland, Sigrid Juselius Foundation, Finnish Cancer Organizations and EMBO Young Investigator Program. A.A. is supported by the Emil Aaltonen foundation, Pertelin Aaltonen foundation, Maud Kuistila foundation and TUBS Graduate School. J.G.L is supported by a fellowship from the Swedish Cancer Society. This study was in part performed at the Live Cell Imaging Unit, Department of Biosciences and Nutrition at Karolinska Institutet, supported by grants from the Knut and Alice Wallenberg Foundation, the Swedish Research Council, and the Center for Biosciences.

Supplementary material available online at
http://jcs.biologists.org/cgi/content/full/123/20/3525/DC1

References

Barbero, P., Bittova, L. and Pfeffer, S. R. (2002). Visualization of Rab9-mediated vesicle transport from endosomes to the trans-Golgi in living cells. *J. Cell Biol.* **156**, 511-518.

Barroso-Gonzalez, J., Machado, J. D., Garcia-Exposito, L. and Valenzuela-Fernandez, A. (2009). Moesin regulates the trafficking of nascent clathrin-coated vesicles. *J. Biol. Chem.* **284**, 2419-2434.

Berg, J. S. and Cheney, R. E. (2002). Myosin-X is an unconventional myosin that undergoes intrafilopodial motility. *Nat. Cell Biol.* **4**, 246-250.

Berg, J. S., Derfler, B. H., Pennisi, C. M., Corey, D. P. and Cheney, R. E. (2000). Myosin-X, a novel myosin with pleckstrin homology domains, associates with regions of dynamic actin. *J. Cell Sci.* **113**, 3439-3451.

Bohil, A. B., Robertson, B. W. and Cheney, R. E. (2006). Myosin-X is a molecular motor that functions in filopodia formation. *Proc. Natl. Acad. Sci. USA* **103**, 12411-12416.

Bolte, S. and Cordelieres, F. P. (2006). A guided tour into subcellular colocalization analysis in light microscopy. *J. Microsc.* **224**, 213-232.

Chen, L., Janetopoulos, C., Huang, Y. E., Iijima, M., Borleis, J. and Devreotes, P. N. (2003). Two phases of actin polymerization display different dependencies on PI(3,4,5)P3 accumulation and have unique roles during chemotaxis. *Mol. Biol. Cell* **14**, 5028-5037.

Cohen, L. A., Honda, A., Varnai, P., Brown, F. D., Balla, T. and Donaldson, J. G. (2007). Active Arf6 recruits ARNO/cytohesin GEFs to the PM by binding their PH domains. *Mol. Biol. Cell* **18**, 2244-2253.

Costes, S. V., Daelemans, D., Cho, E. H., Dobbin, Z., Pavlakis, G. and Lockett, S. (2004). Automatic and quantitative measurement of protein-protein colocalization in live cells. *Biophys. J.* **86**, 3993-4003.

Cox, D., Berg, J. S., Cammer, M., Chinegwundoh, J. O., Dale, B. M., Cheney, R. E. and Greenberg, S. (2002). Myosin X is a downstream effector of PI(3)K during phagocytosis. *Nat. Cell Biol.* **4**, 469-477.

Dent, E. W., Kwiatkowski, A. V., Mebane, L. M., Philippar, U., Barzik, M., Rubinson, D. A., Gupton, S., Van Veen, J. E., Furman, C., Zhang, J. et al. (2007). Filopodia are required for cortical neurite initiation. *Nat. Cell Biol.* **9**, 1347-1359.

Ding, A., Chen, B., Fuortes, M. and Blum, E. (1996). Association of mitogen-activated protein kinases with microtubules in mouse macrophages. *J. Exp. Med.* **183**, 1899-1904.

Fox, J. E. (1985). Identification of actin-binding protein as the protein linking the membrane skeleton to glycoproteins on platelet plasma membranes. *J. Biol. Chem.* **260**, 11970-11977.

Gerhardt, H., Golding, M., Fruttiger, M., Ruhrberg, C., Lundkvist, A., Abramsson, A., Jeltsch, M., Mitchell, C., Alitalo, K., Shima, D. et al. (2003). VEGF guides angiogenic sprouting utilizing endothelial tip cell filopodia. *J. Cell Biol.* **161**, 1163-1177.

Gomes, A. Q., Ali, B. R., Ramalho, J. S., Godfrey, R. F., Barral, D. C., Hume, A. N. and Seabra, M. C. (2003). Membrane targeting of Rab GTPases is influenced by the prenylation motif. *Mol. Biol. Cell* **14**, 1882-1899.

Gould, G. W. and Lippincott-Schwartz, J. (2009). New roles for endosomes: from vesicular carriers to multi-purpose platforms. *Nat. Rev. Mol. Cell Biol.* **10**, 287-292.

Halet, G. (2005). Imaging phosphoinositide dynamics using GFP-tagged protein domains. *Biol. Cell* **97**, 501-518.

Harrison, R. E., Bucci, C., Vieira, O. V., Schroer, T. A. and Grinstein, S. (2003). Phagosomes fuse with late endosomes and/or lysosomes by extension of membrane protrusions along microtubules: role of Rab7 and RILP. *Mol. Cell. Biol.* **23**, 6494-6506.

Insall, R. H. and Weiner, O. D. (2001). PIP3, PIP2, and cell movement-similar messages, different meanings? *Dev. Cell* **1**, 743-747.

Isakoff, S. J., Cardozo, T., Andreev, J., Li, Z., Ferguson, K. M., Abagyan, R., Lemmon, M. A., Aronheim, A. and Skolnik, E. Y. (1998). Identification and analysis of PH domain-containing targets of phosphatidylinositol 3-kinase using a novel in vivo assay in yeast. *EMBO J.* **17**, 5374-5387.

Johnson, C. M., Chichili, G. R. and Rodgers, W. (2008). Compartmentalization of phosphatidylinositol 4,5-bisphosphate signaling evidenced using targeted phosphatases. *J. Biol. Chem.* **283**, 29920-29928.

Kerber, M. L., Jacobs, D. T., Campagnola, L., Dunn, B. D., Yin, T., Sousa, A. D., Quintero, O. A. and Cheney, R. E. (2009). A novel form of motility in filopodia revealed by imaging myosin-X at the single-molecule level. *Curr. Biol.* **19**, 967-973.

Klopfenstein, D. R., Tomishige, M., Stuurman, N. and Vale, R. D. (2002). Role of phosphatidylinositol(4,5)bisphosphate organization in membrane transport by the Unc104 kinesin motor. *Cell* **109**, 347-358.

Knight, P. J., Thirumurugan, K., Xu, Y., Wang, F., Kalverda, A. P., Stafford, W. F., 3rd, Sellers, J. R. and Peckham, M. (2005). The predicted coiled-coil domain of myosin 10 forms a novel elongated domain that lengthens the head. *J. Biol. Chem.* **280**, 34702-34708.

Larkin, M. A., Blackshields, G., Brown, N. P., Chenna, R., McGettigan, P. A., McWilliam, H., Valentin, F., Wallace, I. M., Wilm, A., Lopez, R. et al. (2007). Clustal W and Clustal X version 2.0. *Bioinformatics* **23**, 2947-2948.

Lebrand, C., Corti, M., Goodson, H., Cosson, P., Cavalli, V., Mayran, N., Faure, J. and Gruenberg, J. (2002). Late endosome motility depends on lipids via the small GTPase Rab7. *EMBO J.* **21**, 1289-1300.

Lemmon, M. A. (2004). Pleckstrin homology domains: not just for phosphoinositides. *Biochem. Soc. Trans.* **32**, 707-711.

Lemmon, M. A. and Ferguson, K. M. (2000). Signal-dependent membrane targeting by pleckstrin homology (PH) domains. *Biochem. J.* **350**, 1-18.

Lemmon, M. A., Ferguson, K. M., O'Brien, R., Sigler, P. B. and Schlessinger, J. (1995). Specific and high-affinity binding of inositol phosphates to an isolated pleckstrin homology domain. *Proc. Natl. Acad. Sci. USA* **92**, 10472-10476.

Luikart, B. W., Zhang, W., Wayman, G. A., Kwon, C. H., Westbrook, G. L. and Parada, L. F. (2008). Neurotrophin-dependent dendritic filopodial motility: a convergence on PI3K signaling. *J. Neurosci.* **28**, 7006-7012.

Manna, D., Bhardwaj, N., Vora, M. S., Stahelin, R. V., Lu, H. and Cho, W. (2008). Differential roles of phosphatidylserine, PtdIns(4,5)P2, and PtdIns(3,4,5)P3 in plasma membrane targeting of C2 domains. Molecular dynamics simulation, membrane binding, and cell translocation studies of the PKCalpha C2 domain. *J. Biol. Chem.* **283**, 26047-26058.

Marshall, A. J., Krahn, A. K., Ma, K., Duronio, V. and Hou, S. (2002). TAPP1 and TAPP2 are targets of phosphatidylinositol 3-kinase signaling in B cells: sustained plasma membrane recruitment triggered by the B-cell antigen receptor. *Mol. Cell. Biol.* **22**, 5479-5491.

Mashanov, G. I., Tacon, D., Peckham, M. and Molloy, J. E. (2004). The spatial and temporal dynamics of pleckstrin homology domain binding at the plasma membrane measured by imaging single molecules in live mouse myoblasts. *J. Biol. Chem.* **279**, 15274-15280.

Nagy, S., Ricca, B. L., Norstrom, M. F., Courson, D. S., Brawley, C. M., Smithback, P. A. and Rock, R. S. (2008). A myosin motor that selects bundled actin for motility. *Proc. Natl. Acad. Sci. USA* **105**, 9616-9620.

Niedergang, F. and Chavrier, P. (2004). Signaling and membrane dynamics during phagocytosis: many roads lead to the phagos(R)ome. *Curr. Opin. Cell Biol.* **16**, 422-428.

Nishio, M., Watanabe, K., Sasaki, J., Taya, C., Takasuga, S., Iizuka, R., Balla, T., Yamazaki, M., Watanabe, H., Itoh, R. et al. (2007). Control of cell polarity and motility by the PtdIns(3,4,5)P3 phosphatase SHIP1. *Nat. Cell Biol.* **9**, 36-44.

Oikawa, T., Yamaguchi, H., Itoh, T., Kato, M., Ijuin, T., Yamazaki, D., Suetsugu, S. and Takenawa, T. (2004). PtdIns(3,4,5)P3 binding is necessary for WAVE2-induced formation of lamellipodia. *Nat. Cell Biol.* **6**, 420-426.

Palamidessi, A., Frittoli, E., Garre, M., Faretta, M., Mione, M., Testa, I., Diaspro, A., Lanzetti, L., Scita, G. and Di Fiore, P. P. (2008). Endocytic trafficking of Rac is required for the spatial restriction of signaling in cell migration. *Cell* **134**, 135-147.

Park, W. S., Heo, W. D., Whalen, J. H., O'Rourke, N. A., Bryan, H. M., Meyer, T. and Teruel, M. N. (2008). Comprehensive identification of PIP3-regulated PH domains from C. elegans to H. sapiens by model prediction and live imaging. *Mol. Cell* **30**, 381-392.

Pellinen, T., Arjonen, A., Vuoriluoto, K., Kallio, K., Fransen, J. A. and Ivaska, J. (2006). Small GTPase Rab21 regulates cell adhesion and controls endosomal traffic of beta1-integrins. *J. Cell Biol.* **173**, 767-780.

Quinn, M. T., Parkos, C. A., Walker, L., Orkin, S. H., Dinauer, M. C. and Jesaitis, A. J. (1989). Association of a Ras-related protein with cytochrome b of human neutrophils. *Nature* **342**, 198-200.

Rzomp, K. A., Scholtes, L. D., Briggs, B. J., Whittaker, G. R. and Scidmore, M. A. (2003). Rab GTPases are recruited to chlamydial inclusions in both a species-dependent and species-independent manner. *Infect. Immunol.* **71**, 5855-5870.

Sbalzarini, I. F. and Koumoutsakos, P. (2005). Feature point tracking and trajectory analysis for video imaging in cell biology. *J. Struct. Biol.* **151**, 182-195.

Schober, J. M., Komarova, Y. A., Chaga, O. Y., Akhmanova, A. and Borisy, G. G. (2007). Microtubule-targeting-dependent reorganization of filopodia. *J. Cell Sci.* **120**, 1235-1244.

Shaner, N. C., Campbell, R. E., Steinbach, P. A., Giepmans, B. N., Palmer, A. E. and Tsien, R. Y. (2004). Improved monomeric red, orange and yellow fluorescent proteins derived from Discosoma sp. red fluorescent protein. *Nat. Biotechnol.* **22**, 1567-1572.

Sun, Y., Sato, O., Ruhnow, F., Arsenault, M. E., Ikebe, M. and Goldman, Y. E. (2010). Single-molecule stepping and structural dynamics of myosin X. *Nat. Struct. Mol. Biol.* **17**, 485-491.

Tacon, D., Knight, P. J. and Peckham, M. (2004). Imaging myosin 10 in cells. *Biochem. Soc. Trans.* **32**, 689-693.

Tokuo, H., Mabuchi, K. and Ikebe, M. (2007). The motor activity of myosin-X promotes actin fiber convergence at the cell periphery to initiate filopodia formation. *J. Cell Biol.* **179**, 229-238.

Toyoshima, F. and Nishida, E. (2007). Integrin-mediated adhesion orients the spindle parallel to the substratum in an EB1- and myosin X-dependent manner. *EMBO J.* **26**, 1487-1498.

van Rossum, D. B., Patterson, R. L., Sharma, S., Barrow, R. K., Kornberg, M., Gill, D. L. and Snyder, S. H. (2005). Phospholipase Cgamma1 controls surface expression of TRPC3 through an intermolecular PH domain. *Nature* **434**, 99-104.

Varnai, P. and Balla, T. (2006). Live cell imaging of phosphoinositide dynamics with fluorescent protein domains. *Biochim. Biophys. Acta* **1761**, 957-967.

Varnai, P., Rother, K. I. and Balla, T. (1999). Phosphatidylinositol 3-kinase-dependent membrane association of the Bruton's tyrosine kinase pleckstrin homology domain visualized in single living cells. *J. Biol. Chem.* **274**, 10983-10989.

Weber, K. L., Sokac, A. M., Berg, J. S., Cheney, R. E. and Bement, W. M. (2004). A microtubule-binding myosin required for nuclear anchoring and spindle assembly. *Nature* **431**, 325-329.

Wilcke, M., Johannes, L., Galli, T., Mayau, V., Goud, B. and Salamero, J. (2000). Rab11 regulates the compartmentalization of early endosomes required for efficient transport from early endosomes to the trans-golgi network. *J. Cell Biol.* **151**, 1207-1220.

Woolner, S., O'Brien, L. L., Wiese, C. and Bement, W. M. (2008). Myosin-10 and actin filaments are essential for mitotic spindle function. *J. Cell Biol.* **182**, 77-88.

Yu, C., Feng, W., Wei, Z., Miyanoiri, Y., Wen, W., Zhao, Y. and Zhang, M. (2009). Myosin VI undergoes cargo-mediated dimerization. *Cell* **138**, 537-548.

Zhang, H., Berg, J. S., Li, Z., Wang, Y., Lang, P., Sousa, A. D., Bhaskar, A., Cheney, R. E. and Strömblad, S. (2004). Myosin-X provides a motor-based link between integrins and the cytoskeleton. *Nat. Cell Biol.* **6**, 523-531.

Zhu, G., Chen, J., Liu, J., Brunzelle, J. S., Huang, B., Wakeham, N., Terzyan, S., Li, X., Rao, Z., Li, G. et al. (2007a). Structure of the APPL1 BAR-PH domain and characterization of its interaction with Rab5. *EMBO J.* **26**, 3484-3493.

Zhu, X. J., Wang, C. Z., Dai, P. G., Xie, Y., Song, N. N., Liu, Y., Du, Q. S., Mei, L., Ding, Y. Q. and Xiong, W. C. (2007b). Myosin X regulates netrin receptors and functions in axonal path-finding. *Nat. Cell Biol.* **9**, 184-192.